(ANPA Conference 2024)
ISSN: 2392-473X(Print), 2738-9537 (Online)
Research Article ©Nepal Physical Society
DOI: https://doi.org/10.3126/jnphyssoc.v10i1.72835

Ionospheric Variations in South Korea during the March and April 2023 Geomagnetic Storms

Lok Nath Sharma,[1, 2, a)] Purna Jyoti Shakya,[3, 2, b)] Binod Adhikari,[3, c)] Andres Calabia,[4, d)] and Ananta Panthi[5, e)]

[1)]*Department of Physics, Patan Multiple Campus, IoST, Tribhuvan University, Nepal.*
[2)]*Central Department of Physics, IoST, Tribhuvan University, Nepal*
[3)]*Department of Physics, Patan Multiple Campus, Tribhuvan University, Nepal.*
[4)]*Department of Physics and Mathematics, University of Alcala, Alcalá de Henares, Spain*
[5)]*Department of Physics, Butwal Multiple Campus, IoST, Tribhuvan University, Nepal*

[a)]*Electronic mail: lok.sharma@pmc.tu.edu.np*
[b)]*Electronic mail: purna.shakya@pmc.tu.edu.np*
[c)]*Corresponding author: binod.adhi@gmail.com*
[d)]*Electronic mail: andres@calabia.com*
[e)]*Electronic mail: ananta.panthi@bmc.tu.edu.np*

Abstract. The magnetic reconnection between the Interplanetary Magnetic Field (IMF) and the Earth's magnetic field is the main driver of solar energy input to generate geomagnetic storms. In this work, we employ data from the Global Ionospheric Radio Observatory (GIRO) to study the effects of the March and April 2023 geomagnetic storms on ionospheric Total Electron Content (TEC) and F2 layer critical frequency (foF2) over the Jeju Island, South Korea. We investigate the possible ionospheric connection to solar wind parameters through cross-correlation and continuous wavelet transforms (CWT) analyses. Total electron content and foF2 show a positive correlation above 0.9 to solar wind proton density (Nsw) without time-lag during both storms. On the other side, during the storm of March 2023, TEC and foF2 show a negative correlation of 0.8 to the IMF By component with a time-lag of one hour, while the IMF Bz component and the geomagnetic SYM-H index show a negative correlation of 0.85 and 0.95, respectively without time lag. Conversely, during the storm of April 2023, the correlation of the IMF Bx component to TEC and foF2 are positive with a value of 0.7 with a time-lag of 2.4 hours, while the IMF By and Bz components show a negative correlation to SYM-H around 0.9 with absence of time-lag. These results show the significant fluctuations in ionospheric parameters over Jeju Island, South Korea and emphasizes the sensitivity and importance of ionosphere to space weather monitoring for understanding and mitigating the detrimental effects on communication and navigation systems.

Received: August 28, 2024; **Revised**: October 14, 2024; **Accepted**: October 29, 2024

Keywords: Interplanetary Magnetic Field, Geomagnetic Storm, Ionosphere, Cross-Correlation, Continuous Wavelet Transform.

INTRODUCTION

The magnetic reconnection between the Interplanetary Magnetic Field (IMF) and the Earth's magnetic field is the main driver of solar energy input to generate geomagnetic storms. Geomagnetic storm produces large changes in magnetospheric convection currents. The current and field in the equatorial and low latitude change due to direct penetration of electric field [1], which affect ionospheric plasma distribution. As a result of this disturbance, there is a dramatic change in electron density of F region of the ionosphere. The ionosphere being a dispersive medium, change in electron density or total Electron Content (TEC) affects the radio signal propagation that causes error in GPS communication [2]. TEC is affected by different geographic locations and solar events like solar flare, geomagnetic storm, etc. [3]. The electrodynamical coupling of magnetosphere with solar events and incoming solar radiation directly affect the properties of ionosphere. Energetic electrons of solar and magnetospheric origin, and solar extreme ultraviolet radiation energizes and ionizes the molecules and atoms in the ionosphere. Ionospheric variation plays crucial role in satellite tracking, navigation, radio wave propagation,

etc. [4], hence, its study is essential. Some of the useful parameters to understand ionospheric variations are peak electron density of F2 layer plasma (NmF2), critical frequency of F2 layer (foF2), and TEC [5]. The increase and decrease in these parameters are respectively referred as positive and negative storm effects [6]. In addition, latitude, local time, and the storm's phase determine when and how much of the positive and negative storm effects occur.

In recent years, research has focused on the effects of storm-time electrodynamics, neutral winds, and the ensuing compositional changes [7]. Apart from this, several theoretical and observational investigations have been conducted on storm time ionospheric responses [8, 9]. The association of geomagnetic storms with TEC enhancements has been reported from the low latitudes [10] as well as mid-latitudes [11]. According to Liu et al. [12], seasons, magnetic local times, and magnetic latitudes all affect how long it takes for TEC reactions to occur after geomagnetic disturbances. Study of foF2 variability in the ionosphere is important to improve ionospheric models, such as the International Reference Ionosphere (IRI) [13]. The fluctuation of ionospheric foF2 in the African equatorial latitudes was examined by Akala et al. [14], who concluded that equatorial foF2 variability rises with decreasing solar activity throughout the night. Kuznetsov et al. [15] state that there are differences in the universal variability of foF2 during years of solar minima and maxima.

In this work, we employ data from the Global Ionospheric Radio Observatory (GIRO) to study the effects of the March and April 2023 geomagnetic storms of solar cycle 25, on ionospheric TEC and foF2 over the Jeju Island (33.43° N, 126.3° E), South Korea. The station is located in northern mid-latitude. We chose Jeju Island for our research because it is located at mid-latitude in the northern hemisphere, making it an ideal location for observing geomagnetic disturbances and ionospheric changes. Jeju Island's limited industrial activity results in lower levels of air pollution compared to mainland South Korea. This makes the island an ideal place for upper atmospheric studies related to space weather. Monitoring and studying the variations of TEC and foF2 during geomagnetic storms enhances the ability to predict, prepare for, and mitigate the impacts of geomagnetic storms on human technology and infrastructure.

We investigate the possible ionospheric connection to solar wind data through cross-correlation and continuous wavelet transforms (CWT) analyses to determine the most representative indices and discuss the potential connections during storm-time events.

DATA AND METHODS

Two geomagnetic storms during solar cycle 25 are investigated: the geomagnetic storm of 23-24 March, 2023, and the geomagnetic storm of 23-24 April, 2023. The two storms were chosen based on values of disturbance storm time index (Dst), minimum Dst for March and April storms are -163 nT and -213 nT respectively. On the Dst scale, minor storms have a range of -30 nT to -50 nT, moderate storms have a range of -50 nT to -100 nT, intense storms have a range of -100 nT to -250 nT, and superstorms have a Dst value below -250 nT [16]. The Dst index is estimated from a network of geomagnetic observatories located near to equatorial region and quantifies the strength of the equatorial electrojet, a symmetrical global current that forms a ring around the Earth. Geomagnetic storms lead to the amplification of the ring current, resulting in a significant decrease in the strength of the geomagnetic field. The TEC and the foF2 data over Jeju Island, South Korea (Lat=33.43° N, Long=126.3° E) are obtained from the GIRO repository (https://giro.uml.edu/didbase/scaled.php.). Solar wind parameters and geomagnetic indices are taken from OMNIWeb data explorer (https://omniweb.gsfc.nasa.gov/form/omni_min.html).

In this study, we used the cross-correlation analysis to investigate the correlation of TEC and foF2 with solar wind parameters. Cross-correlation is a method used to determine the connection between two-time series. It is used to determine how the two series match up with each other and at what point the best match occurs. It helps in identifying lagged effects, such as when one variable influences another after a certain delay. Consider two-time series, xi and yi; the cross-correlation r(d) at delay d is defined as [17],

$$r(d) = \frac{\sum_i [(x_i - \bar{x})(y_{i-d} - \bar{y})]}{\sqrt{\sum_i (x_i - \bar{x})^2} \sqrt{\sum_i (y_{i-d} - \bar{y})^2}}, \qquad (1)$$

where i = 0,1, 2, ..., (N-1) and $\bar{x}$, $\bar{y}$ are means of corresponding series.

We also employ the continuous wavelet transform (CWT) to analyse the non-stationary signals in TEC and foF2, where a continuous time function is divided into wavelets [18]. The CWT is a signal processing tool that analyzes and represents non-stationary signals in both time and frequency domains simultaneously. It reveals how frequency content changes over time, making it useful for non-stationary signals. CWT offers high resolution for high frequencies and low resolution for low frequencies, making it ideal for analyzing signals with rapid and slow changes. It is effective in detecting transient features

like spikes, edges, and discontinuities. The CWT of the time series f(t) is determined by the integral transform [19].

$$W_f^{\psi}(a,b) = \int_{-\infty}^{+\infty} f(t) \quad \psi_{a,b}^{\star}(t)dt. \tag{2}$$

In this equation, $\psi_{a,b}^{*}(t)$ is the complex conjugate of the mother wavelet function given by

$$\psi_{a,b}(t) = \frac{1}{\sqrt{a}}\psi\left(\frac{t-b}{a}\right). \tag{3}$$

where a and b are scale and translational parameters which represent the scale and time localization of the wavelet function.

RESULTS AND DISCUSSION

The geomagnetic storm of 23-24 March, 2023 was generated from a combined effect of a co-rotating interaction region (CIR) and a coronal mass ejection (CME) occurring on 20-21 March, 2023 [20]. The storm started at G3 (strong) level at 14:40 UTC on 23 March and reached a peak level of G4 (severe) at 04:16 UTC on 24 March. G-scale is used by National Oceanic and Atmospheric Administration (NOAA) to measure strength of geomagnetic storm. The storm kept the Earth's magnetic field disturbed for more than 21 continuous hours. Figure 1 shows the IMF components Bx, By, Bz (in GSM), and SYM-H index and the solar wind velocity (Vsw), solar wind proton density (Nsw), and solar wind plasma pressure (Psw) parameters during the storm of 23-24 March, 2023. In this figure, denoted with a vertical red line, we observe the Sudden Storm Commencement (SSC) occurring at about 06:30 UTC on 23 March, indicating an increase in SYM-H.

During the main phase of the storm, Bz turns southward at -16.82 nT, SymH reduced to -170 nT, solar wind velocity (Vsw) increased to 509 km/s, solar wind proton density (Nsw) increased to 42.27 n/cc, and solar wind plasma pressure (Psw) increased to 22.75 nPa. According to Tsurutani et al. [21], the main source of strong magnetic storms is the very large values of southward directed IMF Bz.

The geomagnetic storm of 23-24 April, 2023 was a G4 level storm, originated by a coronal mass ejection (CME) associated with an M1.7 solar flare that erupted on 21 April [22]. The SSC of the storm is clearly seen in Figure 2 at 08:56 UTC, 23 April, with an enhanced SYM-H, solar wind proton density, and solar wind plasma pressure. After the SSC, the Bz is oriented southward and reduces to – 25 nT, then, the Bz is directed northward with maximum value reaching to 31.5 nT, and turns southward to -33 nT few hours later. During this storm, the Sym-H is reduced to -233 nT, the Vsw increased to 748.6 km/s, the Nsw increased to 30.25 n/cc, and the Psw increased to 19.5 nPa.

Dungey [23] and Cowley [24] suggested the southward IMF can re-connect with the geomagnetic field and develop geomagnetic storms. The size of Bz going southern from northward is greatly reliant on the severity of the storm, and variations in F2 layer parameters during a geomagnetic storm are significantly dependent on the storm strength [25]. A comprehensive examination of the ionosphere's responses reveals that during storms, F2 values dropped simultaneously in the equatorial and mid-latitude regions. Low to moderate changes in ionospheric F2 during the pre-storm period may also indicate the impending arrival of major ionospheric disturbances during the main phase. The ionospheric F2 reaction at low and mid-latitudes does not differ significantly between the main phase of storm and the pre-storm period.

Figure 3 shows variation of TEC and foF2 during the geomagnetic storm of 23-24 March, 2023. Before SSC both TEC and foF2 show normal diurnal pattern, with minimum values before sunrise and the values slowly increase and become maximum at noon. Peak values of TEC and foF2 are 49.3 TECU and 13.925 MHz respectively. During the period of storm both TEC and foF2 show depletion, both at night side and day side. Figure 4 shows variation of TEC and foF2 during geomagnetic storm of 23-24 April. Both TEC and foF2 have the same pattern as in 23-24 March storm. Peak values of TEC and foF2 before storm are 47.3 TECU and 12.575 MHz respectively. During the period of storm both TEC and foF2 show depletion, having peak values of 33.7 TECU and 7.6 MHz respectively, at local noon time.

During a geomagnetic storm, the increased energy and momentum in the upper atmosphere at higher altitudes cause heating via Joule heating. This leads to changes in the thermospheric contents and the formation of moving atmospheric disturbances, which move towards the equator. This leads to changes in the density, composition, circulation, and dynamics of the ionosphere-thermosphere system, which causes fluctuations in the total electron content (TEC) and electron plasma densities [26]. Prompt penetration electric fields are the primary factor driving the positive ionospheric storm phase, while the negative ionospheric storm phase occurs in the midlatitude region due to a combination of factors including the equatorward shift of midlatitude density trough, disturbance dynamo electric fields, compression of the plasmapause in the equatorial region, and changes in chemical configuration [27].

Figure 5 shows the correlation of TEC and foF2 with solar wind parameters and geomagnetic index during storm of 23-24 March, 2023. TEC and foF2 show positive correlation of about 0.95 with Nsw, with no time

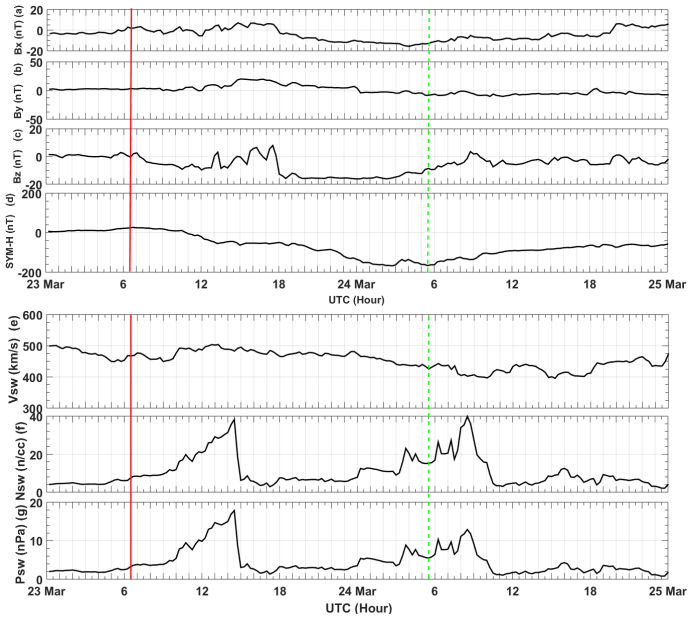

FIGURE 1: Solar wind parameters during geomagnetic storm of 23-24 March, 2023. From top to bottom, we show the (a) X-component of IMF, (b) Y-component of IMF, (c) Z-component of IMF, (d) Symmetric H-component (SYM-H) index (e) solar wind velocity, (f) solar wind proton density, and the (g) solar wind plasma pressure. Vertical red line indicates SSC and dash green line indicates end of main phase of storm.

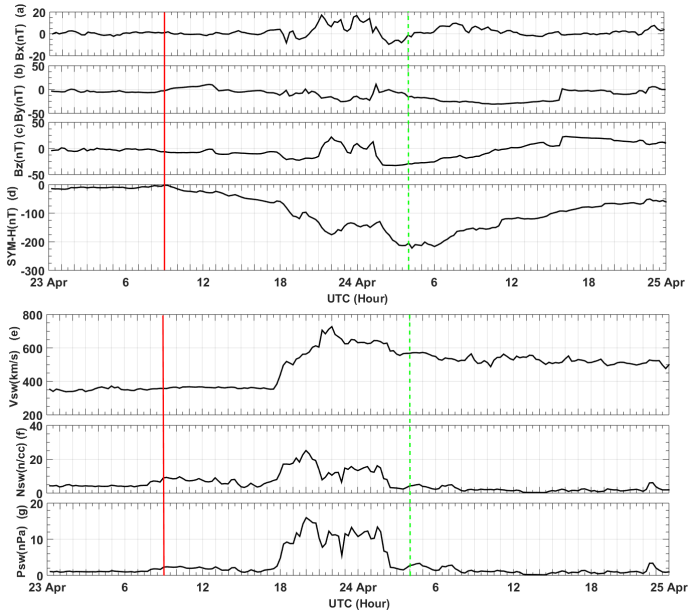

FIGURE 2: Solar wind parameters during geomagnetic storm of 23-24 April, 2023. From top to bottom, we show the (a) X-component of IMF, (b) Y-component of IMF, (c) Z-component of IMF, (d) Symmetric H-component (SYM-H) index (e) solar wind velocity, (f) solar wind proton density, and the (g) solar wind plasma pressure. Vertical red line indicates SSC and dash green line indicates end of main phase of storm.

lag. However, TEC and foF2 show negative correlation of range 0.75 to 0.95 with IMF components and geomagnetic index,with no time lag to time lag of 1 hour. Figure 6 shows correlation of TEC and foF2 with solar wind parameters and geomagnetic index during storm of 23-24 April, 2023. TEC and foF2 show positive correlation of

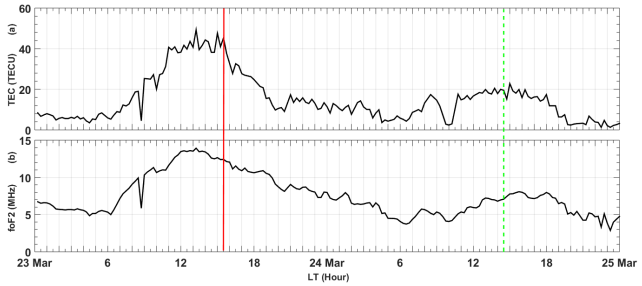

FIGURE 3: Variations in (a) TEC, and (b) foF2, in Local Time (LT) during 23-24 March, 2023. Vertical red line indicates SSC and green line indicates end of main phase of storm in LT.

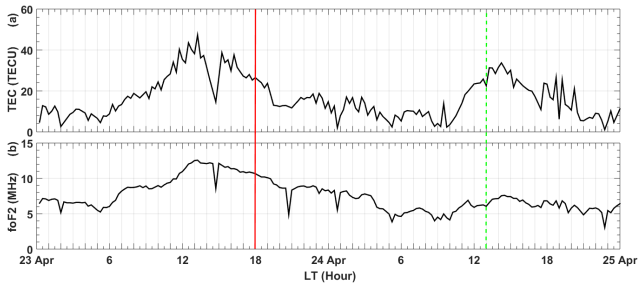

FIGURE 4: Variations in (a) TEC, and (b) foF2, in Local Time (LT) during 23-24 April, 2023. Vertical red line indicates SSC and green line indicates end of main phase of storm in LT.

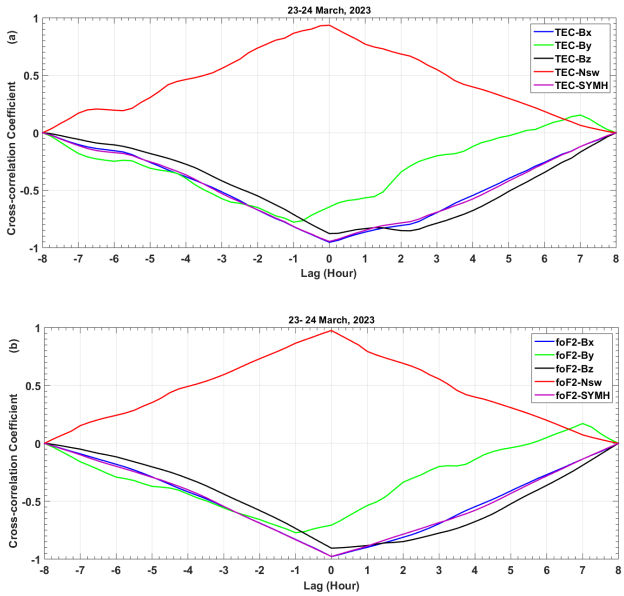

FIGURE 5: Correlations-delay plots (a) TEC and solar wind parameters, (b) foF2 and solar wind parameters, during 23-24 March, 2023.

about 0.95 with Nsw, with no time lag, and of 0.7 with IMF-Bx component with negative time lag of 2.3 hours. However, TEC and foF2 show negative correlation of range 0.8 to 1 with IMF y and z-components, By and Bz, respectively and SymH, with no time lag. These results show that during the period of storm both TEC and foF2 show depletion, due to a various factors such as the equatorward shift of midlatitude density trough, disturbance dynamo electric fields, compression of the plasmapause in the equatorial region.

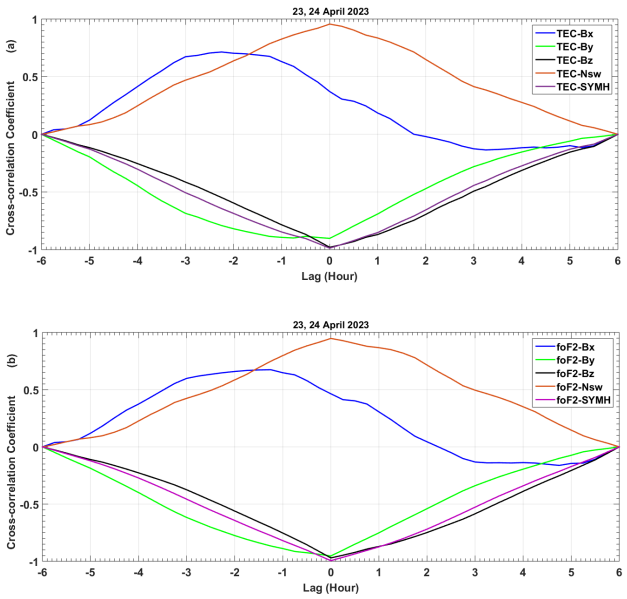

FIGURE 6: Correlations-delay plots (a) TEC and solar wind parameters, (b) foF2 and solar wind parameters, during 23-24 April, 2023.

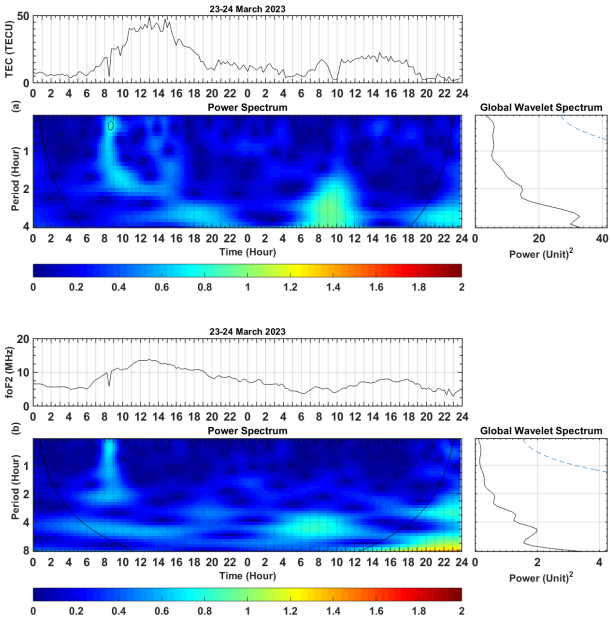

FIGURE 7: Wavelet scalogram of (a) TEC and (b) foF2, during storm of 23-24 March, 2023.

Figure 7 shows the result of the scalogram of TEC and foF2, during storm of 23-24 March, 2023. In the scalogram of TEC, there is strong wavelet power density of about 32 units, of low frequency, from 06:00 LT to 12:00 LT, on March 24. In the scalogram of foF2 there is strong wavelet power density of about 2 units, of low frequency, from 03:00 LT to 11:00 LT, on March 24. Figure 8 shows the result of the scalogram of TEC and foF2, during storm of 23-24 April, 2023. In the scalogram of TEC there are very strong wavelet power density of about 145 units, of low frequency, from 09:00 LT to 20:00 LT, on April 23, and again from 07:00 LT to 15:00 LT, on 24 April. In the scalogram of foF2, there are strong wavelet power density of about 4 units, of low frequency, from 07:00 LT to 13:00 LT, on April 23, and again from 01:00 LT to 10:00 LT, on 24 April. Power areas of high and low intensities

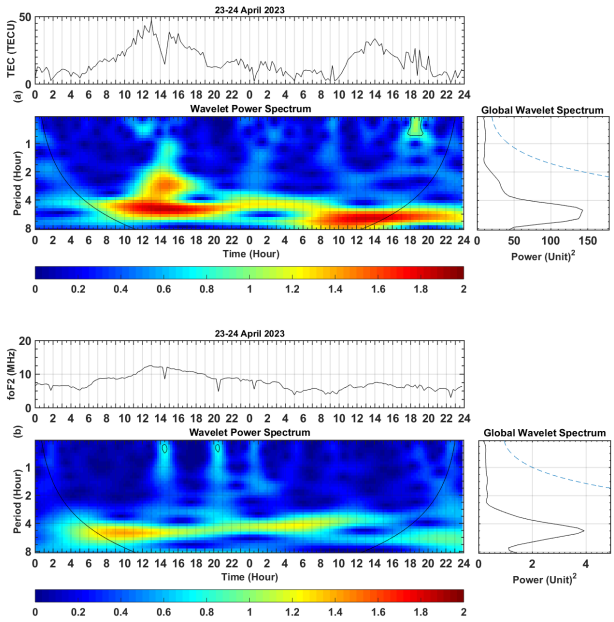

FIGURE 8: Wavelet scalogram of (a) TEC and (b) foF2, during storm of 23-24 April, 2023.

at different times and scales in the scalogram show the variation of TEC and foF2 during storm periods. High intensity and low frequency indicate large variation of TEC and foF2 at slower rate, while high intensity and high frequency signifie large variations at faster rate. Changes in TEC and foF2 during geomagnetic storms have a significant negative impact on navigation and communication systems by causing delays, mistakes, and signal loss. In order to minimize these impacts and ensure the safety and reliability of these systems, real-time monitoring and predictive modeling of space weather are essential.

CONCLUSIONS

The main conclusions from our study are as given:

- There is depletion in TEC and foF2 during periods of both storms of March and April, 2023. It is due to Joule heating which leads to changes in the thermospheric contents and the movement of atmospheric disturbances towards the equator. It changes the density, composition, circulation, and dynamics of the ionosphere-thermosphere system, which causes fluctuations in the total electron content (TEC) and electron plasma densities [28].
- TEC and foF2 show good positive correlation with solar wind proton density (Nsw) with no time lag, during storm periods. However, TEC and foF2 show negative correlation with SymH (geomagnetic index), and components of IMF. This can be attributed to the fact that negative ionospheric storm phase occurs in the midlatitude region due to the equatorward shift of midlatitude density trough, disturbance dynamo electric fields, compression of the plasmapause in the equatorial region, and changes in chemical configuration [29].
- CWT analysis of TEC and foF2 show strong power density during periods of both storms. The maximum wavelet power on the scalogram corresponds to high peaks on the global wavelet spectrum. Time-frequency analysis of TEC and foF2 during storm provides frequency and location of the event in the time series.

ACKNOWLEDGMENTS

The data for solar wind parameters and geomagnetic indices was taken from: https://omniweb.gsfc.nasa.gov/form/omni_min.html.The data for ionospheric TEC and foF2 layer were taken from: https://giro.uml.edu/didbase/scaled.php.

EDITORS' NOTE

This manuscript was submitted to the Association of Nepali Physicists in America (ANPA) Conference 2024 for publication in the special issue of the Journal of Nepal Physical Society.

REFERENCES

1. J. Sastri, M. Abdu, and J. Sobral, "Response of equatorial ionosphere to episodes of asymmetric ring current activity," in *Annales Geophysicae*, Vol. 15 (Springer, 1997) pp. 1316–1323.
2. R. Tiwari, S. Bhattacharya, P. Purohit, and A. Gwal, "Effect of tec variation on gps precise point at low latitude," The open atmospheric science journal **3** (2009).
3. A. A. Mansoori, P. A. Khan, R. Ahmad, R. Atulkar, A. Aslam, S. Bhardwaj, B. Malvi, P. Purohit, and A. Gwal, "Evaluation of long term solar activity effects on gps derived tec," in *Journal of Physics: Conference Series*, Vol. 759 (IOP Publishing, 2016) p. 012069.
4. O. Maltseva and N. Mozhaeva, "Obtaining ionospheric conditions according to data of navigation satellites," International Journal of Antennas and Propagation **2015**, 804791 (2015).
5. O. Maltseva, "The influence of space weather on the relationship between the parameters tec and fof2 of the ionosphere," IEEE Journal of Radio Frequency Identification **5**, 261–268 (2021).
6. M. J. Buonsanto, "Ionospheric storms—a review," Space Science Reviews **88**, 563–601 (1999).
7. T. J. Fuller-Rowell, "Storm-time response of the thermosphere–ionosphere system," Aeronomy of the Earth's Atmosphere and Ionosphere , 419–435 (2011).
8. I. Kutiev, I. Tsagouri, L. Perrone, D. Pancheva, P. Mukhtarov, A. Mikhailov, J. Lastovicka, N. Jakowski, D. Buresova, E. Blanch, *et al.*, "Solar activity impact on the earth's upper atmosphere," Journal of Space Weather and Space Climate **3**, A06 (2013).
9. B. Zhao, W. Wan, L. Liu, K. Igarashi, K. Yumoto, and B. Ning, "Ionospheric response to the geomagnetic storm on 13–17 april 2006 in the west pacific region," Journal of Atmospheric and Solar-Terrestrial Physics **71**, 88–100 (2009).
10. P. Galav, S. Sharma, and R. Pandey, "Response of low latitude ionosphere to the geomagnetic storm of may 30," Astrophysics and Space Science **337**, 543–551 (2012).
11. S. Basu, S. Basu, E. MacKenzie, C. Bridgwood, C. Valladares, K. Groves, and C. Carrano, "Specification of the occurrence of equatorial ionospheric scintillations during the main phase of large magnetic storms within solar cycle 23," Radio Science **45**, 1–15 (2010).
12. J. Liu, B. Zhao, and L. Liu, "Time delay and duration of ionospheric total electron content responses to geomagnetic disturbances," in *Annales Geophysicae*, Vol. 28 (Copernicus GmbH, 2010) pp. 795–805.
13. D. Bilitza, L.-A. McKinnell, B. Reinisch, and T. Fuller-Rowell, "The international reference ionosphere today and in the future," Journal of Geodesy **85**, 909–920 (2011).
14. A. Akala, E. Oyeyemi, E. Somoye, A. Adeloye, and A. Adewale, "Variability of fof2 in the african equatorial ionosphere," Advances in space research **45**, 1311–1314 (2010).
15. K. VV, P. VV, N. GV, and N. II, "Universal variation of the f2-layer critical frequency and solar activity," Earth, planets and space **50**, 57–61 (1998).
16. W. Gonzalez, J.-A. Joselyn, Y. Kamide, H. W. Kroehl, G. Rostoker, B. Tsurutani, and V. Vasyliunas, "What is a geomagnetic storm?" Journal of Geophysical Research: Space Physics **99**, 5771–5792 (1994).
17. P. Bourke, "Cross correlation," Cross Correlation", Auto Correlation—2D Pattern Identification **596** (1996).
18. A. Grossmann and J. Morlet, "Decomposition of hardy functions into square integrable wavelets of constant shape," SIAM journal on mathematical analysis **15**, 723–736 (1984).
19. D. Sonechkin and N. Datsenko, "Wavelet analysis of nonstationary and chaotic time series with an application to the climate change problem," Fractals and Dynamic Systems in Geoscience , 653–677 (2000).
20. A. Tahir, F. Wu, M. Shah, C. Amory-Mazaudier, P. Jamjareegulgarn, T. G. Verhulst, and M. A. Ameen, "Multi-instrument observation of the ionospheric irregularities and disturbances during the 23–24 march 2023 geomagnetic storm," Remote Sensing **16**, 1594 (2024).
21. B. T. Tsurutani, W. D. Gonzalez, F. Tang, and Y. T. Lee, "Great magnetic storms," Geophysical Research Letters **19**, 73–76 (1992).
22. A. Elmhamdi, A. Marassi, P. Romano, L. Contarino, W. AlShehri, and C. Monstein, "The multifaceted m1. 7 goes-class flare event of 21 april 2023 in ar13283," Solar Physics **299**, 109 (2024).
23. J. W. Dungey, "Interplanetary magnetic field and the auroral zones," Physical Review Letters **6**, 47 (1961).
24. S. W. Cowley, "Plasma populations in a simple open model magnetosphere," Space Science Reviews **26**, 217–275 (1980).
25. B. Adekoya, V. Chukwuma, N. Bakare, and T. David, "On the effects of geomagnetic storms and pre storm phenomena on low and middle latitude ionospheric f2," Astrophysics and Space Science **340**, 217–235 (2012).
26. M. Mendillo, "Storms in the ionosphere: Patterns and processes for total electron content," Reviews of Geophysics **44** (2006).
27. C. Nayak, L.-C. Tsai, S.-Y. Su, I. Galkin, A. T. K. Tan, E. Nofri, and P. Jamjareegulgarn, "Peculiar features of the low-latitude and midlatitude ionospheric response to the st. patrick's day geomagnetic storm of 17 march 2015," Journal of Geophysical Research: Space Physics **121**, 7941–7960 (2016).
28. W. Li, D. Zhao, J. Feng, X. Wu, and Z. Zhang, "Spatial development of strong storm-induced ionospheric perturbations during 25–27 august 2018," Remote Sensing **15**, 2549 (2023).
29. I. Horvath, "Impact of 10 january 1997 geomagnetic storm on the nighttime weddell sea anomaly: A study utilizing data provided by the topex/poseidon mission and the defense meteorological satellite program, and simulations generated by the coupled thermosphere/ionosphere plasmasphere model," Journal of Geophysical Research: Space Physics **112** (2007).
30. B. G. Fejer, "Low latitude ionospheric electrodynamics," Space Science Reviews **158**, 145–166 (2011).